Journal of
Materials Chemistry A

Accepted Manuscript

This article can be cited before page numbers have been issued, to do this please use: S. Huang, J. Song, Y. Lu, C. Lv, H. Zheng, X. Liu, Z. Jin, D. Zhao, C. J. Carmalt and I. P. Parkin, *J. Mater. Chem. A*, 2016, DOI: 10.1039/C6TA04908G.

This is an *Accepted Manuscript*, which has been through the Royal Society of Chemistry peer review process and has been accepted for publication.

Accepted Manuscripts are published online shortly after acceptance, before technical editing, formatting and proof reading. Using this free service, authors can make their results available to the community, in citable form, before we publish the edited article. We will replace this *Accepted Manuscript* with the edited and formatted *Advance Article* as soon as it is available.

You can find more information about *Accepted Manuscripts* in the Information for Authors.

Please note that technical editing may introduce minor changes to the text and/or graphics, which may alter content. The journal's standard Terms & Conditions and the Ethical guidelines still apply. In no event shall the Royal Society of Chemistry be held responsible for any errors or omissions in this *Accepted Manuscript* or any consequences arising from the use of any information it contains.

ROYAL SOCIETY OF CHEMISTRY

www.rsc.org/materialsA

View Article Online
DOI: 10.1039/C6TA04908G

Journal Name

ARTICLE

Power-Free Water Pump Based on Superhydrophobic Surface: Generation of Mushroom-Like Jet and Anti-Gravity Long-Distance Transport

Received 00th January 20xx,
Accepted 00th January 20xx

DOI: 10.1039/x0xx00000x

www.rsc.org/

Shuai Huang [a], Jinlong Song [a]*, Yao Lu [b], Cunjing Lv [c], Huanxi Zheng [a], Xin Liu [a], Zhuji Jin [a], Danyang Zhao [a], Claire J. Carmalt [b], Ivan P. Parkin [b]

Spontaneously anti-gravitational transportation of liquids in a long distance is widely discovered in nature, such as the water transportation from the root to the crown of a tree. However, it remains a challenge to artificial liquid delivery. In this work, a new power-free pump composed of a superhydrophobic plate with a pore mounted on a leak-proof cylinder container filled with water is presented for sustained anti-gravity and long distance transport. Water droplets can be spontaneously captured through the pore by the lower water column, forming a mushroom-like jet due to the energy transition from surface energy to kinetic energy. The spontaneously increased inside pressure in the container will push the water out, through another thin tube, realizing the energy transition from surface energy to gravity potential energy. The dynamic driving and moving model of the pivotal mushroom-like jet was analyzed. The maximum transport height and transport ability of water pump were also discussed. The results show that Laplace pressure is the main driving pressure of the mushroom-like jet and that the developed power-free pump which can effectively transport water to over 100 mm height with an average transport speed of 4500 $\mu L \cdot h^{-1}$, showing an application potential in the microfluidic system and medical devices where micro pump is needed.

1. Introduction

In our daily life, pumps are widely used to transport water upward or to a distant place. A lot of energy is consumed by the power pump to attain sustained transportation. Moreover, unexpected power outage for especial pump will have potentially risks. For example, if the insulin pump stopped unwittingly, it would cause unpredictable harm to patients. Hence the development of a power-free method to transport liquid would be of considerable benefit. In nature, the most famous power-free pump system are trees, which can transport water from its roots to the crown via the trunk due to the capillary, transpiration and osmotic effects [1]. Many biological surfaces also process this similar function [2-5]. O'Leary's study reveals that the water transport in some plants is mainly driven by capillary force and negative xylem pressure [6]. Inspired by nature, researchers are looking for new methods to realize the power-free anti-gravity and long-distance transport of water. Methods reported previously for the anti-gravity transport of water include thermally driven pump [7], chemically driven methods [8, 9], surface tension driven methods [10-16], and various other approaches [17-21]. Delamarche et al [22-24] developed a capillary pump for use in biological analysis, where the high precision transport of nano-fluid was realized. Bush et al [25, 26] studied the foraging strategies of bird beakes, and proposed that transport of millimetric droplets could be motivated by a combination of surface tension and a capillary ratchet. Megaridis et al [27] developed microfluidic platform driven by surface tension and realized anti-gravity transport to a height of 10 mm. Cao et al [28] used a superhydrophobic mesh to develop a surface tension driven pump which could spontaneously and continuously deliver water to a maximum height of 14 mm. Although some achievements have been obtained in the area of power-free water pump, unfavorable features such as low transport height, low transport velocity, and difficulties with long distance transport demonstrate the significant challenges to meet practical application.

In the past decades, surfaces with extreme wettability showed good application potential in the manipulation of droplets, transport of macro/nano-fluids, and coalescence of droplets, biological analysis, and oil/water separation [29-34]. Here, we developed a power-free water-pump composed of a superhydrophobic plate with a pore mounted on a leak-proof cylinder container filled with water. The plate employed shows excellent superhydrophobicity on both sides. When a water

[a] Key Laboratory for Precision and Non-Traditional Machining Technology of Ministry of Education, Dalian University of Technology, Dalian 116024, China. Corresponding author: Jinlong Song; *Email: songjinlong@dlut.edu.cn
[b] Materials Chemistry Research Centre, Department of Chemistry, University College London, 20 Gordon Street, London, WC1H 0AJ, UK.
[c] Center of Smart Interfaces, Technische Universität Darmstadt, Darmstadt 64287, Germany.
Electronic Supplementary Information (ESI) available: see DOI: 10.1039/x0xx00000x

View Article Online
DOI: 10.1039/C6TA04098C

droplet is dropped on the pore, the lower water will absorb the droplet and result in a release of surface energy. Surface energy will be transferred into kinetic energy first, forming a mushroom-like jet, then further into gravitational potential energy, realizing the anti-gravity and long-distance transport through another thin tube. This work presents a novel water delivery system with a transport height of hundred millimeters scale, and should serve as a source to design advanced devices, sensors and actuators in the fields of microfluidics and lower-energy industry.

2. Experimental

2.1 Fabrication of the wettability plates.

The pure Al plate (thickness, 0.4 mm) are hydrophilic; after etching by 1 mol·L^{-1} aqueous $CuCl_2$ solution for 20 s, the Al plate was transformed into a superhydrophilic material; when the etched Al plate was immersed in the 0.05 mol·L^{-1} ethanol solution of stearic acid (STA) for 20 min, it was transferred into a superhydrophobic surface. Before chemical etching, the pore on the sample surface was drilled by a precision bench drill (ZX7016, Yisong, China). The apparent contact angle (CA), microscopic morphology, and chemical composition of the samples were measured by optical CA meter (DSA100, Krüss, Germany), scanning electron microscopy (SEM, SUPRA 55 SAPPHIRE, Germany), and energy-dispersive X-ray spectroscope (EDS, SUPRA 55 SAPPHIRE, Germany), respectively. In the experiment, water was dyed red for better visualization. The self-capturing process was observed by a high-speed colour camera (HotShot 512 SC, Japan).

2.2 Characterization of the wettability plates.

The results of wettability, microscopic morphology and main chemical compositions of the Al surfaces obtained at the different processing conditions are shown in Fig.1. The uncoated Al surface was very smooth and showed hydrophilicity with a contact angle of 72° ± 3°, and the smooth structure was considered to be a layer of oxides due to the Al and O elements detected by EDS spectrum [Fig. 1 (a)]. After $CuCl_2$ etching, the Al surface was covered by micro/nanometer-scale Al structures composed of irregularly rectangular pits and protrusions, here surface features increase the contact area of the solid-liquid and results in superhydrophilicity with a contact angle of 4° ± 1.5° [Fig. 1 (b)]. After modification with stearic acid, the surface energy of the micro/nanometer-scale Al structures were reduced. The combination of rough structures and low surface energy contributes to the surface superhydrophobicity with a contact angle of 158°± 2° [Fig. 1 (c)]. The EDS spectra indicate the presence of C and O due to the stearic acid added to the surface.

2.3 Properties of the water pump.

The water pump was a cylindrical tube with a body external diameter of 30 mm, an internal diameter of 27 mm and a length of 110 mm. The material composition of the pumps and tubes were Plexiglas and Teflon, respectively. The water droplet was supplied by a syringe.

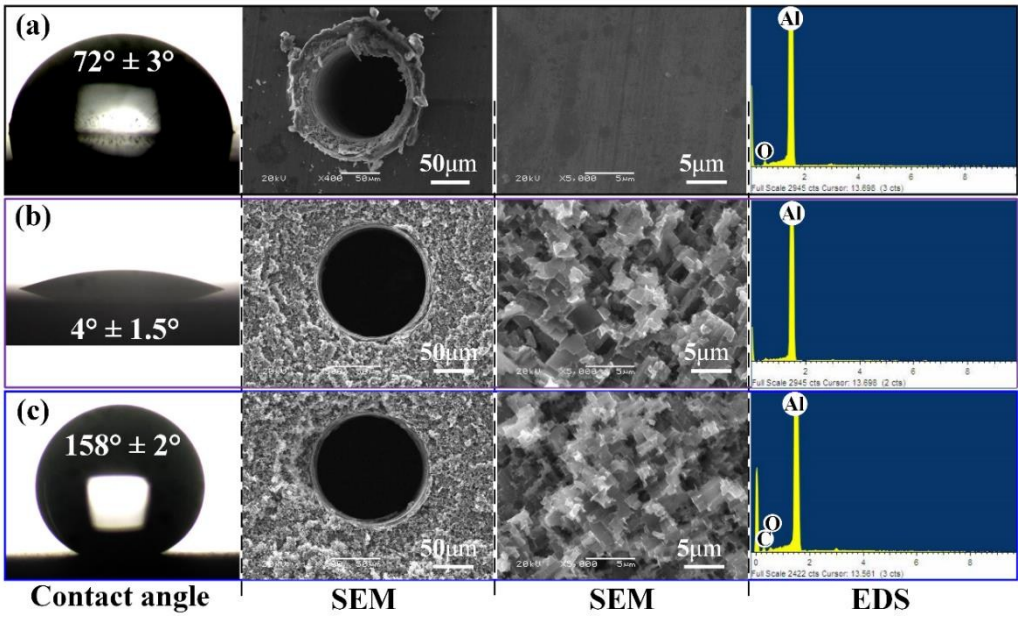

Fig. 1 Wettability, microscopic morphology and main chemical compositions of the Al surfaces (pore diameter, 0.1 mm) under the different processing conditions: (a) hydrophilic surface obtained from ordinary Al surface, (b) superhydrophilic surface obtained from $CuCl_2$ etched Al surface, and (c) superhydrophobic surface fabricated by $CuCl_2$ etching and stearic acid modification.

3. Results and discussion

3.1 Generation of mushroom-like jet.

For an open environment, when a water droplet is dropped into water, the droplet would be spontaneously captured by the water surface and coalesce into the bulk, evolving to a ring, as shown in Fig. 2 (a). If a thin plate with a pore is put on the water

View Article Online
DOI: 10.1039/C6TA04098C

surface and then the water droplet is dropped on the pore, the situation changes drastically, as shown in Figs. 2 (b) to 2 (d). The bottom side of the water droplet could touch the lower water and then be captured by coalescence, forming a jet. This phenomenon is known as a self-capturing process. We also observed that the shape of the jet was different when using plates with different wettability. For superhydrophilic and hydrophilic plates, the jets were very weak [Figs. 2 (b) and 2 (c)]. However, for the superhydrophobic plate, the jet was very strong with a straight moving track and fast moving velocity, looking like a mushroom with long tail [Fig. 2 (d) and Movie S1 of Supporting Information].

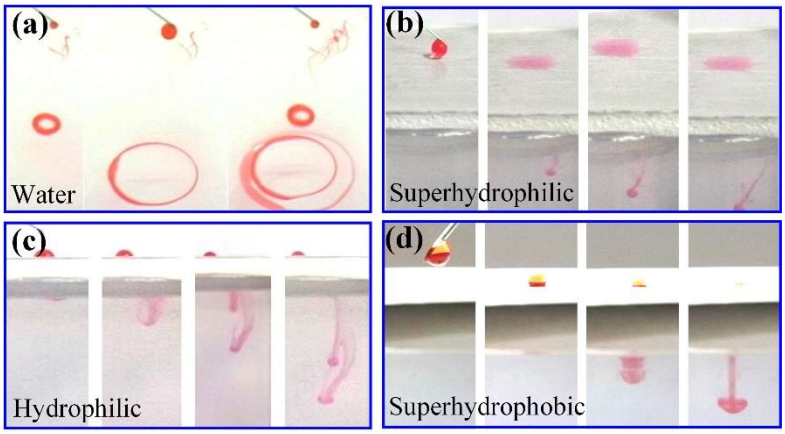

Fig. 2 (a) The free expansion process of a water droplet on water. The penetration process of water droplets on the pore of (b) superhydrophilic surface, (c) hydrophilic surface and (d) superhydrophobic surface. The volume of water droplet is ~ 6.4 μL.

To visualize the self-capturing process of the water droplet on superhydrophobic plate, a high-speed colour camera was employed for the real-time observance of the penetration process. The water droplet is in an unstable state with a gradually reduced contact angle [Fig.3 (a), Fig. S1 and Movie S2 of Supporting Information]. Figs. 3 (b) and 3 (c) display the model of the self-capturing process of a water droplet on the superhydrophobic plate. Before the instantaneous volume V_i of the water droplet was larger than the critical volume V_{cri}, which refers to when the contact line just reduced to the pore diameter (Table S1, Supporting Information), although the solid-liquid contact line shrank and the radius R_i of water droplet decreases with the decreasing of droplet volume V_i [Fig. 3 (b)], the instantaneous contact angle θ_i of the water droplet remained constant and was equal with the initial contact angle θ_i of about 158°. In contrast, when $V_i \le V_{cri}$, the solid-liquid contact line pinned on the pore rather than further shrinking. In this case, θ_i gradually decreased with the droplet volume V_i [Fig. 3 (c)], satisfies $R_i = r/\sin\theta_i$, where r is the radius of the pore. The instantaneous volume V_i of these two stages can be calculated as

$$V_i = \begin{cases} \frac{1}{3}\pi R_i^3(2-3\cos\theta_0+\cos^3\theta_0), & V_i \ge V_{cri} \\ \frac{1}{3}\pi\left(\frac{r}{\sin\theta_i}\right)^3(2-3\cos\theta_i+\cos^3\theta_i), & V_i \le V_{cri} \end{cases} \quad (1)$$

Fig. 3 (d) gives the relationship between contact angle and the volume of water droplets under different pore sizes measured by dropping water droplets with different volumes. The fluctuation trend of the contact angle in the experimental was in agreement with the theoretical model.

During the self-capturing process, the formation of the mushroom-like jet and the shrinking of the droplet were driven by the Laplace pressure $\Delta P = 2\gamma/R_i$. On the basis of Equation (1), ΔP can be derived as follows:

$$\Delta P = \begin{cases} 2\gamma[\frac{\pi(2-3\cos\theta_0+\cos^3\theta_0)}{3V_i}]^{1/3}, & V_i \ge V_{cri} \\ \frac{2\gamma\sin\theta_i}{r}, & V_i \le V_{cri} \end{cases} \quad (2)$$

where γ is the surface tension of water at room temperature, 72.8 mN·m^{-1}. According to Equation (2), the plot of Laplace pressure ΔP is shown in Fig. 3 (e). For different pore diameters, when the $V_i \ge V_{cri}$, the decrease of V_i resulted in a slowly increased ΔP. When $V_i \le V_{cri}$, the decrease of V_i and θ_i resulted in an increased ΔP and was followed by a decrease. The maximal ΔP was obtained when the contact angle was 90°.

The driving force F_L of the self-capturing process resulting from the Laplace pressure can be calculated as $F_L = \Delta P \cdot S$, where $S = \pi r^2$ denotes the section area of the pore. With a decrease of V_i and θ_i, F_L increases first and then decreases [Fig. 3 (f)].

The geometric centroid of the spherical-cap-shape water droplet during the self-capturing process occurs at a distance z above the plate and is given by

$$z = \frac{1}{4}\cdot\frac{(1-\cos\theta_i)(3+\cos\theta_i)}{(2+\cos\theta_i)}R_i \quad (3)$$

During coalescence of the droplet with the bulk, the geometric centroid z is shown a decreasing continuously [Fig. 3 (g)]. To quantify the shrinking rate of the droplet, the instantaneous acceleration a_i of the centroid of the water droplet can be simply estimated as $a_i \sim F_L/\rho V_i$ based on the momentum conservation, in which ρ is the mass density of water. The corresponding plot of a_i as a function of V_i exhibited a similar trend at different pore radius [Fig. 3 (h)]. The initial

acceleration increased gradually and was followed by a dramatic growth, allowing the generation of the sustained mushroom-like jet. Furthermore, we measured the moving length of the mushroom-like jet, as shown in Fig. 3 (i), the experimental length-time ($L \sim t^{1/2}$) profiles of the mushroom-like jet were approximately linear.

After the water droplet was captured by water pump, the evolution process on hydrodynamics mechanisms of mushroom-like jet was similar to that of the plunging liquid jet, a water column impacting on the free surface of a liquid reservoir after penetrating an ambient atmosphere [35-38].

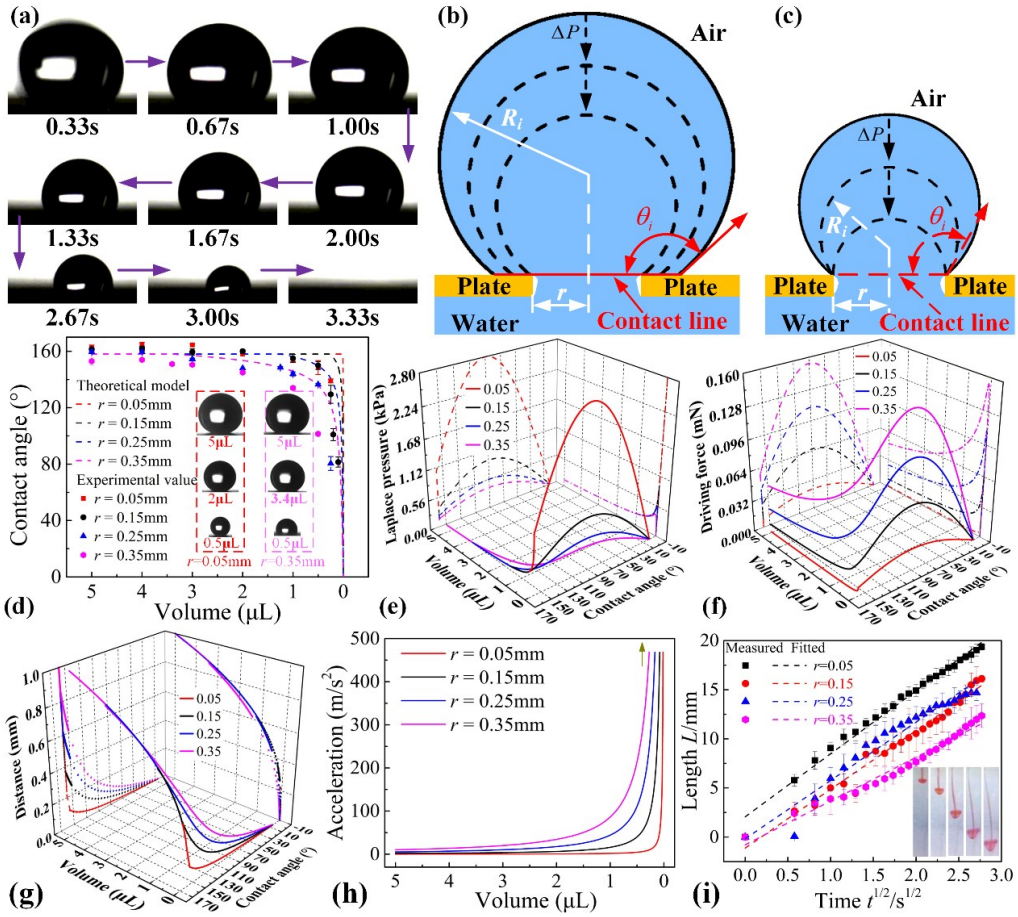

Fig. 3 (a) Time-lapsed images of water CA in the capturing process (r = 0.05 mm). (b - c) Schematic diagram of self-capturing process (ΔP is the Laplace pressure. R_i and θ_i are the instantaneous radius and CA, respectively. r is the pore radius). (d) The influence of volume of water droplet on CA under different pore sizes. (e) Instantaneous Laplace pressure, (f) driving force and (g) distance of the geometric centroid of spherical-cap-shape water droplet as a function of CA and volume at different pores radius (mm). (h) The plot of instantaneous acceleration of water droplet during self-capturing process with a varied volume. (i) Variation of jet length with the time at different pores radius (mm).

The aforementioned dynamic analysis indicates that the single droplet can penetrate the pore on the thin plate via Laplace pressure and then is captured by the water surface to generate a mushroom-like jet without any external power. The water entering into a sealed container filled with water causes a spontaneous increase of the internal pressure. If a tube is added on the side of a container, this pressure can provide a driving force to pump water out, forming a power-free pump, and realizing the transition from surface energy to gravity potential energy, which is the essential feature of this work. A superhydrophobic plate with multiple pores was fabricated to generate multiple mushroom-like jets, which could improve the transport efficiency (Movie S3 of Supporting Information).

3.2 Power-free water pump.

The adhesion force F_a between the plate and water droplets directly affected the self-capturing process, and was calculated by sliding angles using Equation (4). The experiment of measuring sliding angles was shown in Fig. 4 (a) and Movie S4 of Supporting Information.

$$F_a = F_G = \rho g V \sin\alpha \quad (4)$$

where g represents the gravitational acceleration; V is the volume of droplets; α is the measured sliding angle, F_G is the component of the gravity force along the plate. From Equation (4), it can be seen that the adhesion force for a specific volume is proportional to sinα. The sliding angle of the droplet on a flat superhydrophobic surface without pores was only 5° [Fig. 4 (b)]. However, the sliding angle became larger with increase of the pore diameter. For example, the sliding angle was up to 35° when the pore diameter was 0.7 mm. For the hydrophilic surface, the experiment results showed that the droplets did not slide down until the plate was tilted to 90° with various diameters. Water residue still remained on the pore inlet of the hydrophilic surface after the self-capturing process [Fig. 4 (c2)]. However, for the superhydrophilic surface, water spread quickly

View Article Online
DOI: 10.1039/C6TA04908G

on the surface without any sliding angle [Fig. 4 (c3)]. Therefore, the minimum adhesion force was obtained on superhydrophobic surface, which was beneficial for the self-capturing process.

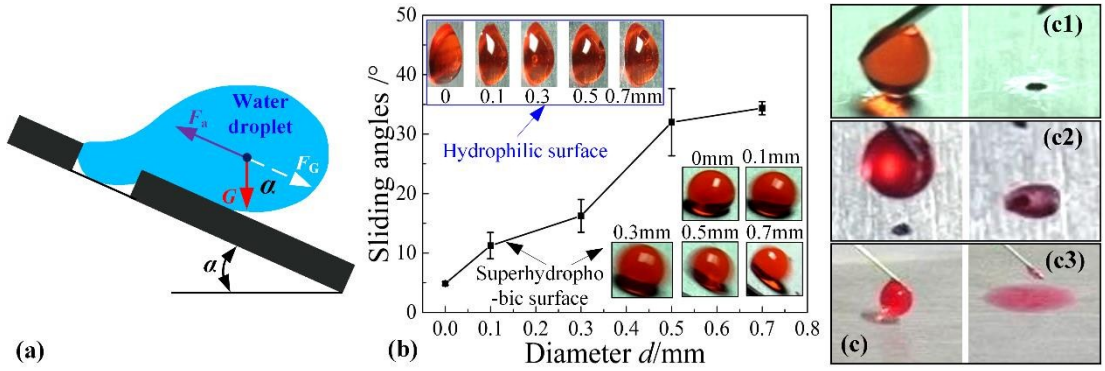

Fig. 4 (a) Schematic of the method to measure sliding angles. (b) Sliding angles of plates with different wettability and diameters. (c) Adhesion state of water droplet at the pore inlet: c1, superhydrophobic surface; c2, hydrophilic surface; c3 superhydrophilic surface (droplet volume is ~6.4 μL).

The cylindrical water pump was designed by using a self-capturing principle via a pore mounted on a leak-proof cylinder container filled with water as shown in Fig. 5 (a). The pressure resisting capacity of the pore directly affects the transport capacity of the water pump. A measuring system containing a plate with a pore and a cylindrical container was employed to measure the pressure resisting capacity, as shown in Fig. 5 (b). Water was poured into the measuring device slowly until it leaked from the pore. The competition between the forces F_p and F_s, resulting from the hydrostatic pressure of the water column and the surface tension along the boundary of the pore, can be expressed as follows:

$$\begin{cases} F_p = \rho g h \cdot \pi (\frac{d}{2})^2 \\ F_s = \gamma \cdot \pi d \left|\cos\theta\right| \end{cases} \quad (5)$$

in which θ_i is the water contact angle; h stands for the height of water column. The maximum pressure resisting h_{max}, which is derived from $F_p = F_s$ and can be expressed as follows:

$$h_{max} = \frac{4\gamma\left|\cos\theta\right|}{\rho g d} \quad (6)$$

Here, it should be noted that additional Laplace pressure rendered by the tube itself was neglected due to the hydrophobic property of the Teflon tubes. According to Equation (6), when the plate contained a superhydrophobic surface with a pore diameter of 0.1 mm, the pressure resisting height was measured to be 229.0 mm. The pressure resisting height was decreased in accordance with the enhancement of pore diameter, as shown in Fig. 5 (c). For the hydrophilic surface, a similar trend was exhibited but the pressure resisting height was a little lower than that of the superhydrophobic surface. However, for the superhydrophilic surface, water spread and leaked quickly from the pore when water was poured into the measuring device, indicating that the superhydrophilic pore did not possess any pressure resisting capacity.

The results above showed that the adhesion force and pressure resisting capacity on the superhydrophobic surface were optimized and of best fit for making the water pump. Utilizing this water pump with a pore diameter of 0.1 mm, water can be lifted to 144.6 mm with an average transport speed of 4500 μL·h^{-1} [Fig.5 (d) and Movie S5 of Supporting Information]. The increase of transportation height h resulted in a dramatic decreased transportation speed and was followed by a decrease trend gradually because the driving pressure was changed (Fig. S2 and Fig. S3 of Supporting Information). In the transport process, it can be seen that the transport height of the pump depends on the F_L and F_h [Fig. 5 (a)]. Where, F_L is the driving force from the Laplace pressure difference [Fig.3 (f)], and arises from an increase of the transport height h_t which resulted in an increasing force of F_h, which generate a pressure ΔP_h and is given by $\Delta P_h = \rho g h_t$. However, it is surprising that the experimentally measured transport height h_t was less than the pressure resisting height h_{max}. The different from the pressure resisting experiment [Figs. 5 (b) and 5 (c)], we speculate, is due to some possible influences such as the uncertainty of the finial contact state between the droplet and the pore because the self-capturing process is a dynamic process, dissipation of energy resulting from the expanding of the container, etc., which suppress the maximum height and makes it hard for us to give a high precision model. This remaining open question is beyond the scope of this manuscript and will be investigated further next in our research program. Combining Equation (2), a prediction model of Equation (7) was obtained to estimate the maximum transport height $h_{t\,max}$ by fitting the experimental data, the results showed that the critical contact angles for the maximum transport height with different pores were different [Fig. 5 (d)].

$$h_{t\,max} = \frac{2\gamma}{\rho g r}\sin(152.3 - 30.6r) \quad (7)$$

View Article Online
DOI: 10.1039/C6TA04908G

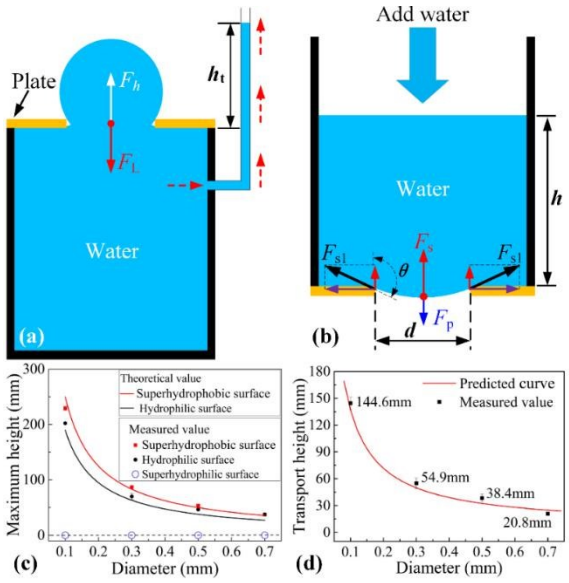

Fig. 5 (a) Principle of water pump. (b) Arrangement for measurement of the pressure resisting capability. (c) Maximum pressure-resisting height of pores with different diameter at different wettabilities. (d) Maximum transport height of water pump with different pore diameters.

3.3 Transport ability of water pump on different posture.

The feasibility of using the superhydrophobic plate to design the water pump was verified in our study, and a transport height on the order of a hundred millimeter scale was achieved. To test the practicality of the water pump, further research was conducted on the transport height under different tube diameters and the pump body with different tilted angles β [Fig. 6 (a)]. The results showed that the transport height was not related to the tube diameter and the pump tilting angle because the water pressure was unchanged inside the pump under the various states [Figs. 6 (b) and 6(c)]. Based on this good stability, an extensive application prospect of the water pump is expected.

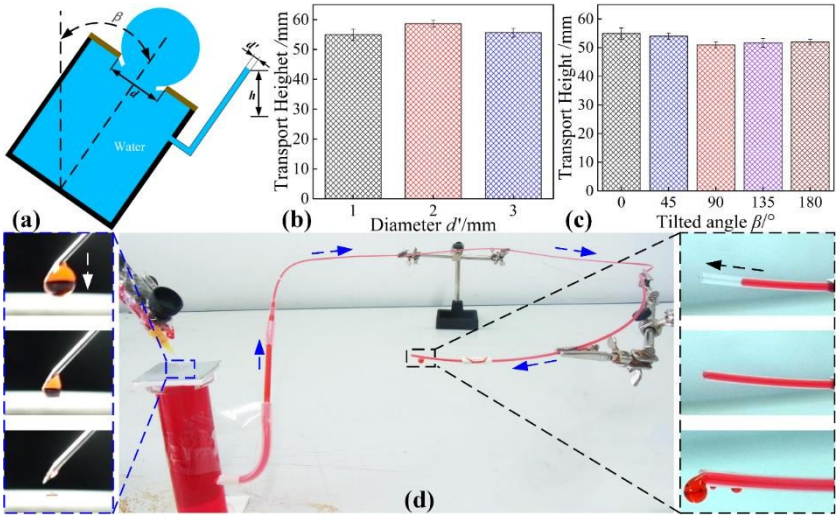

Fig. 6 (a) Transport process of unpowered pump with different posture; transport height of (b) the tube with different diameter d' (no tilted angle), and (c) the unpowered pump with different tilted angles β (pore diameter, 0.3 mm). (d) Long distance transport of liquids (tube length, 1 m; tube diameter, 1 mm; pore diameter, 0.3 mm).

An integrated long distance transport system is displayed in Fig. 6 (d). The pore diameter on the superhydrophobic plate was 0.1 mm and the tube with a length of 1 m was positioned optionally but maintained higher than the upper water surface of the pump. Droplets were consecutively transported along the tube to the outlet tube after being captured by the pump without any external driving force (Movie S6, Supporting Information). If the end of the tube is lower than the level of water surface in the container, before the liquid reaches the peak point of the tube, the Laplace pressure is the main driving force. After the liquid filled with the whole tube, siphon effect will also promote the transportation process besides the Laplace pressure. If the end of the tube is higher than the level of water surface in the container, that situation is not meet the condition of siphon. Thus, Laplace pressure is still the main driving force. In the experiment shown in Fig. 6 (d), the whole

tube is higher than the level of water surface in the container, indicating that the siphon effect can be ignored. The superhydrophobic surface can maintain its function unless the plate is damaged by oil-contamination or mechanical force. The water pump will not lose efficacy in the normal application condition. Therefore, our power-free pump could be employed as a novel device for advanced fluid delivery systems.

Conclusions

A mushroom-like jet with high moving velocity was observed when dropping a water droplet onto the pore of superhydrophobic plates on water surface, showing a high energy transition efficiency from surface energy to gravity potential energy. Based on this self-capturing phenomenon, a power-free water pump composed of a superhydrophobic plate with a pore mounted on a leak-proof cylinder container filled with water was designed to transfer the surface energy into gravity potential energy and this realized the anti-gravity long distance transport of water. The measuring experiments indicate that the superhydrophobic surface with high pressure resisting capacity and low adhesion is the preferable material for designing the power-free water pump. The spontaneous anti-gravity transport height of the pump was up to a hundred millimeters scale and increased with a decrease of the pore diameter. Further study indicated that the transport capacity of the water pump was not affected by the different states, e.g., tilted angle of pump body and tube diameter, which demonstrated that the pump processed good stability. A sustained delivery of water with long distance was achieved using the integrated antigravity transport system. This water pump obtained an anti-gravity transport height with hundred millimeters scale and long distance on the meter scale, and should have potential application in the field of microfluidics system to design advanced devices, sensors and actuators, etc.

Acknowledgment

This work was financially supported by National Natural Science Foundation of China (NSFC, Grant No. 51275071 and No. 51305060) and the Fundamental Research Funds for the Central Universities (DUT15RC(3)066).

References:

1 M. A. Zwieniecki, P. J. Melcher and N. M. Holbrook, *Science*, 2001, **291**, 1059.
2 Y. Zheng, H. Bai, Z. Huang, X. Tian, F. Nie, Y. Zhao, J. Zhai and L. Jiang, *Nature*, 2010, **463**, 640.
3 A. R. Parker and C. R. Lawrence, *Nature*, 2001, **414**, 33.
4 J. Ju, H. Bai, Y. Zheng, T. Zhao, R. Fang and L. Jiang, *Nat Commun*, 2012, **3**, 1247.
5 J. Ju, Y. Zheng and L. Jiang, *Acc. Chem. Res.*, 2014, **47**, 2342.
6 W. T. Pockman, J. S. Sperry and J. W. Oleary, *Nature*, 1995, **378**, 715.
7 R. H. Farahi, A. Passian, T. L. Ferrell and T. Thundat, *Appl Phys Lett*, 2004, **85**, 4237.
8 J. Yong, Q. Yang, F. Chen, H. Bian, G. Du, U. Farooq and X. Hou, *Adv. Mater. Interfaces*, 2015, **2**,.
9 S. T. Plummer and P. W. Bohn, *Langmuir*, 2002, **18**, 4142.
10 A. Nakajima, *Npg Asia Mater*, 2011, **3**, 49.
11 M. K. Chaudhury and G. M. Whitesides, *Science*, 1992, **256**, 1539.
12 A. Y. Vorobyev and C. Guo, *Appl Phys Lett*, 2009, **94**, 224102.
13 C. Wang and T. Hsueh, *J. Phys Chem C.*, 2014, **118**, 12399.
14 S. Huang, J. Song, Y. Lu, F. Chen, H. Zheng, X. Yang, X. Liu, J. Sun, C. J. Carmalt, I. P. Parkin and W. Xu, *ACS Appl. Mater. Interfaces*, 2016, **8**, 2942.
15 C. Lv, P. Hao, Z. Yao, Y. Song, X. Zhang and F. He, *Appl Phys Lett*, 2013, **103**, 21601.
16 C. Lv, C. Chen, Y. C. Chuang, F. G. Tseng, Y. Yin, F. Grey and Q. Zheng, *Appl Phys Lett*, 2014, **113**, 26101.
17 X. Niu, F. Gielen, J. B. Edel and A. J. DeMello, *Nat Chem*, 2011, **3**, 437.
18 M. Grunze, *Science*, 1999, **283**, 41.
19 J. V. I. Timonen, M. Latikka, L. Leibler, R. H. A. Ras and O. Ikkala, *Science*, 2013, **341**, 253.
20 J. Barman, D. Swain, B. M. Law, R. Seemann, S. Herminghaus and K. Khare, *Langmuir*, 2015, **31**, 1231.
21 H. Chen, P. Zhang, L. Zhang, H. Liu, Y. Jiang, D. Zhang, Z. Han and L. Jiang, *Nature*, 2016, **532**, 85.
22 L. Gervais and E. Delamarche, *Lab Chip*, 2009, **9**, 3330.
23 E. Bazzo and M. Nogoseke, *Appl Therm Eng*, 2003, **23**, 1153.
24 M. Zimmermann, H. Schmid, P. Hunziker and E. Delamarche, *Lab Chip*, 2007, **7**, 119.
25 H. W. Krenn, *Annu Rev Entomol*, 2010, **55**, 307.
26 M. Prakash, D. Quere and J. W. M. Bush, *Science*, 2008, **320**, 931.
27 A. Ghosh, R. Ganguly, T. M. Schutzius and C. M. Megaridis, *Lab Chip*, 2014, **14**, 1538.
28 M. Cao, K. Li, Z. Dong, C. Yu, S. Yang, C. Song, K. Liu and L. Jiang, *Adv Funct Mater*, 2015, **25**, 4114.
29 Y. Tian, B. Su and L. Jiang, *Adv Mater*, 2014, **26**, 6872.
30 A. Tuteja, W. Choi, M. Ma, J. M. Mabry, S. A. Mazzella, G. C. Rutledge, G. H. McKinley and R. E. Cohen, *Science*, 2007, **318**, 1618.
31 L. Feng, S. H. Li, Y. S. Li, H. J. Li, L. J. Zhang, J. Zhai, Y. L. Song, B. Q. Liu, L. Jiang and D. B. Zhu, *Adv Mater*, 2002, **14**, 1857.
32 T. Darmanin, E. T. de Givenchy, S. Amigoni and F. Guittard, *Adv Mater*, 2013, **25**, 1378.
33 R. Enright, N. Miljkovic, J. Sprittles, K. Nolan, R. Mitchell and E. N. Wang, *Acs Nano*, 2014, **8**, 10352.
34 J. C. Bird, R. Dhiman, H. Kwon and K. K. Varanasi, *Nature*, 2013, **503**, 385.
35 X. Qu, L. Khezzar and Z. Li, *Proc. Inst. Mech. Eng., Part E*, 2012, **226**, 238.
36 X. Qu, A. Goharzadeh, L. Khezzar and A. Molki, *Exp Therm Fluid Sci*, 2013, **44**, 51.
37 X. L. Qu, L. Khezzar, D. Danciu, M. Labois and D. Lakehal, *Int. J. Multiphase Flow*, 2011, **37**, 722.
38 C. Narayanan and D. Lakehal, *J. Heat Transfer*, 2008,.

View Article Online
DOI: 10.1039/C6TA04908G

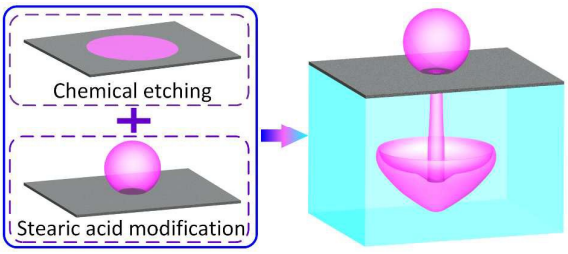

Self-capturing phenomenon was investigated to design an integrated antigravity transport system based on superhydrophobic surface